J. Fluid Mech. (2020), *vol*. 900, R6, doi:10.1017/jfm.2020.565



JFM RAPIDS
journals.cambridge.org/rapids

Café latte: spontaneous layer formation in laterally cooled double diffusive convection

Kai Leong Chong[1,†], **Rui Yang**[1], **Qi Wang**[1,2], **Roberto Verzicco**[1,3,4] **and Detlef Lohse**[1,5,†]

[1]Physics of Fluids Group, Max Planck Center for Complex Fluid Dynamics, MESA+ Institute and J.M.Burgers Center for Fluid Dynamics, University of Twente, P.O. Box 217, 7500 AE Enschede, The Netherlands

[2]Department of Modern Mechanics, University of Science and Technology of China, Hefei 230027, China

[3]Dipartimento di Ingegneria Industriale, University of Rome 'Tor Vergata', Via del Politecnico 1, Roma 00133, Italy

[4]Gran Sasso Science Institute – Viale F. Crispi, 7 67100 L'Aquila, Italy

[5]Max Planck Institute for Dynamics and Self-Organisation, 37077 Göttingen, Germany

(Received 26 April 2020; revised 25 June 2020; accepted 6 July 2020)

In the preparation of café latte, spectacular layer formation can occur between the espresso shot in a glass of milk and the milk itself. Xue *et al.* (*Nat. Commun.*, vol. 8, 2017, pp. 1–6) showed that the injection velocity of espresso determines the depth of coffee–milk mixture. After a while, when a stable stratification forms in the mixture, the layering process can be modelled as a double diffusive convection system with a stably stratified coffee–milk mixture cooled from the side. More specifically, we perform (two-dimensional) direct numerical simulations of laterally cooled double diffusive convection for a wide parameter range, where the convective flow is driven by a lateral temperature gradient while stabilized by a vertical concentration gradient. Depending on the strength of stabilization as compared to the thermal driving, the system exhibits different flow regimes. When the thermal driving force dominates over the stabilizing force, the flow behaves like vertical convection in which a large-scale circulation develops. However, with increasing strength of the stabilizing force, a meta-stable layered regime emerges. Initially, several vertically-stacked convection rolls develop, and these well-mixed layers are separated by sharp interfaces with large concentration gradients. The initial thickness of these emerging layers can be estimated by balancing the work exerted by thermal driving and the required potential energy to bring fluid out of its equilibrium position in the stably stratified fluid. In the layered regime, we further observe successive layer merging, and eventually only a single convection roll remains. We elucidate the following merging mechanism: as weakened circulation leads to accumulation of hot fluid adjacent to the hot sidewall, larger

† Email addresses for correspondence: k.l.chong@utwente.nl, d.lohse@utwente.nl

© The Author(s), 2020. Published by Cambridge University Press. This is an Open Access article, distributed under the terms of the Creative Commons Attribution licence (http://creativecommons.org/licenses/by/4.0/), which permits unrestricted re-use, distribution, and reproduction in any medium, provided the original work is properly cited.

https://doi.org/10.1017/jfm.2020.565 Published online by Cambridge University Press

buoyancy forces associated with hotter fluid eventually break the layer interface. Then two layers merge into a larger layer, and circulation establishes again within the merged structure.

Key words: double diffusive convection

1. Introduction

Layered patterns are striking features in double diffusive convection (DDC), where the fluid density depends on two scalars with different diffusivities (Turner 1974; Huppert & Turner 1981; Schmitt 1994; Radko 2013; Garaud 2018). A typical example of layer formation is found in the ocean, where seawater density is affected by temperature and salinity. As a result of double diffusion, thermohaline staircases are found in different regions of the ocean, such as a salt-finger regime in (sub)tropic regions (Simeonov & Stern 2004; Schmitt 2005; Johnson & Kearney 2009; Yang *et al.* 2020) and a diffusive regime in high-latitude regions (Kelley *et al.* 2003; Timmermans *et al.* 2008; Sommer *et al.* 2013).

An intriguing daily example of layered pattern can be found in café latte, where the corresponding laboratory experiments have recently been conducted by Xue *et al.* (2017). When a shot of espresso (lower-density) is poured into a glass of milk (higher-density), the system cools down from the side since it loses heat to the ambient through the sidewall. Pronounced layers form in the mixture, rather than a mixed-up solution as one may expect. Xue *et al.* (2017) showed that the injection velocity determines the depth of milk being mixed with espresso. After a while when a stably stratified zone forms in the mixture, the layering process is governed by double diffusion: the temperature difference between the hotter bulk and the colder sidewall fluid layer implies a horizontal thermal driving, whereas a stabilizing vertical concentration gradient exists in the coffee–milk mixture.

Examples in other physical systems also illustrate the importance of horizontal thermal driving to layer formation in a stably stratified fluid. For instance, when sedimenting suspensions of colloidal particles are subjected to a horizontal temperature gradient, the initially uniform suspension will also develop multiple layers (Mendenhall & Mason 1923). Also, one can observe layering when ice blocks melt in salty liquid, building up a salinity gradient (Huppert & Turner 1980).

To numerically study layer formation in DDC systems with both vertical and lateral gradients, here we pick, inspired by café latte, laterally cooled double diffusive convection with a concentration gradient in the vertical direction. In this set-up, the temperature gradient is imposed horizontally, whereas the vertical concentration gradient is stabilizing. In pioneering experimental and theoretical work of laterally cooled DDC, Thorpe, Hutt & Soulsby (1969) showed the successive growth of layers in a stratified brine solution heated from one side. They further conducted linear stability analysis to find the onset criteria of layers. Their pioneering paper motivated further experimental and numerical work focusing on how the layers form (Chen, Briggs & Wirtz 1971; Wirtz, Briggs & Chen 1972; Lee & Hyun 1991). Also, salinity and heat fluxes were studied extensively in laterally cooled DDC because it is relevant to the high-latitude ocean being affected by melting icebergs (Huppert & Turner 1980; Jacobs *et al.* 1981; Gayen, Griffiths & Kerr 2016). Moreover, layer merging in DDC is also an important issue because it influences the fluxes across the layer interface (Tanny & Tsinober 1988; Chen & Chen 1997).

Previous simulations (mostly in the 20th century) on DDC had severe CPU-time limitation on the parameter range and on collecting long enough time series of layer

https://doi.org/10.1017/jfm.2020.565 Published online by Cambridge University Press

evolution. Thanks to the full temperature and velocity information obtained from present numerical simulations, the extension of the parameter space and the possibility to run very long simulations, the layer formation and properties can now be understood in much more detail.

In this work, we study laterally cooled DDC over a wide range in parameter space, namely three decades of temperature Rayleigh number Ra_T and four decades of density ratio Λ. We begin with the description of the governing equations and the set-up in § 2. Then we examine the flow morphologies and show the layer formation in § 3. In § 4, we can estimate the thickness of the initially formed layers from an energy balance. We further elucidate the mechanism of layer merging in § 5. Finally, conclusions are given in § 6.

2. Numerical method and set-ups

We consider a two-dimensional rectangular box of width W and height H. The left/right wall has high/low temperature, and there is no salinity flux through the lateral boundaries. The top/bottom wall has low/high salinity and is adiabatic to temperature. No-slip velocity boundary conditions are used on all the walls. We apply the Oberbeck–Boussinesq (OB) approximation, such that the fluid density depends linearly on temperature $\tilde{T}$ and a scalar $\tilde{S}$: $\tilde{\rho}(\tilde{T}, \tilde{S}) = \tilde{\rho}_0[1 - \beta_T(\tilde{T} - \tilde{T}_0) + \beta_S(\tilde{S} - \tilde{S}_0)]$. Here, $\tilde{\rho}_0$, $\tilde{T}_0$, $\tilde{S}_0$ represent the reference density, temperature and concentration, respectively. The thermal and solutal expansion coefficients are β_T and β_S, respectively. The governing equations are non-dimensionalized by normalizing lengths by H, velocities by the free-fall velocity $U = \sqrt{g\beta_T|\Delta_T|H}$ (such that time is non-dimensionalized by the free-fall time scale H/U), temperatures by Δ_T (the temperature difference between the sidewalls) and concentrations by Δ_S (the concentration difference between the top and bottom plates):

$$\partial_t u_i + u_j \partial_j u_i = -\partial_i p + \sqrt{\frac{Pr_T}{Ra_T}} \partial_j \partial_j u_i + (T - \Lambda S)\, \delta_{iz}, \tag{2.1}$$

$$\partial_t T + u_i \partial_i T = \frac{1}{\sqrt{Ra_T Pr_T}} \partial_j^2 T, \tag{2.2}$$

$$\partial_t S + u_i \partial_i S = \frac{1}{Le\sqrt{Ra_T Pr_T}} \partial_j^2 S, \tag{2.3}$$

$$\partial_i u_i = 0. \tag{2.4}$$

Here, u_i/u_j are the velocity components, p the kinematic pressure, T the temperature and S the concentration, all now non-dimensional. The Kronecker delta is denoted by δ_{iz} and the gravitational acceleration by g. The five dimensionless control parameters are the aspect ratio Γ, the thermal Rayleigh Ra_T and the Prandtl Pr_T number for the temperature, the Lewis number Le, and the density ratio Λ, defined as:

$$\Gamma = W/H, \quad Ra_T = \frac{g\beta_T H^3 \Delta_T}{\kappa_T \nu}, \quad Pr_T = \frac{\nu}{\kappa_T}, \tag{2.5a–c}$$

https://doi.org/10.1017/jfm.2020.565 Published online by Cambridge University Press

$$Le = \kappa_T/\kappa_S = Pr_S Pr_T^{-1}, \quad \Lambda = (\beta_S \Delta_S)\,/\,(\beta_T \Delta_T) = Ra_S Ra_T^{-1} Le^{-1}, \tag{2.6a,b}$$

where $Ra_S = g\beta_S H^3 \Delta_S/(\kappa_S \nu)$ is the concentration Rayleigh number and $Pr_S = \nu/\kappa_S$ the concentration Prandtl number. Here, ν, κ_T and κ_S are the kinematic viscosity, the thermal diffusivity and the solutal diffusivity, respectively. The relative strength of the buoyancy force induced by the stabilizing concentration difference to that induced by the destabilizing temperature difference is measured by Λ. The three key response parameters of the system are the two scalar fluxes and the flow velocity, which are measured by the two Nusselt numbers and the Reynolds number:

$$Nu_T = \sqrt{Ra_T Pr_T}\langle u_x T\rangle_{z,t} - \langle \partial_x T\rangle_{z,t}, \tag{2.7}$$

$$Nu_S = \sqrt{Ra_S Pr_S}\langle u_z S\rangle_{x,t} - \langle \partial_z S\rangle_{x,t}, \tag{2.8}$$

$$Re = \sqrt{Ra_T/Pr_T}\sqrt{\langle \boldsymbol{u}^2\rangle}. \tag{2.9}$$

Here $\langle . \rangle_{x,t}/\langle . \rangle_{z,t}$ represents the average over time and the horizontal/vertical plane. In this work, we calculate Nu_T by temperature gradients at the two sidewalls and Nu_S by concentration gradients at the top and bottom plates. The root-mean-square value of the velocity magnitude, calculated over the entire domain, is $\sqrt{\langle \boldsymbol{u}^2\rangle}$.

Equations (2.1)–(2.4) are solved by a second-order finite difference scheme using a fractional-step procedure and advanced in time by a low-storage third-order Runge–Kutta scheme (Verzicco & Orlandi 1996; van der Poel *et al.* 2015). We use fixed aspect ratio $\Gamma = 0.5$. We have also conducted a case of aspect ratio 1 for $Ra_T = 10^7$ and $Ra_S = 2 \times 10^9$, which also shows the successive layer merging and eventually a single convection roll. Our simulations cover the range $10^6 \leq Ra_T \leq 10^9$, $10^{-2} \leq \Lambda \leq 10^2$ with $Pr_T = 1$ and $Pr_S = 100$ (corresponding to a Lewis number $Le = 100$). Although in the café latte problem, Le is approximately 10^3, Le considered in this study is large enough to demonstrate the layer formation. The large Le implies that the resolution for the concentration is more demanding than that for the temperature, and thus a multiple resolutions strategy is employed (Ostilla-Mónico *et al.* 2015), and such strategy had been already used for DDC simulations (Yang, Verzicco & Lohse 2015). Specifically, for the case of $Ra_T = 10^9$, we use 432^2 for the base mesh and 1296^2 for the refined mesh. Uniform grid spacing is adopted horizontally while stretched grid spacing is adopted vertically with more grid points near the top and bottom walls. We also ensure that there are enough grid points to capture the sharp concentration gradient between the layers. Besides, a grid independence test has been conducted to ensure that the same final conclusion has been obtained when the grid size is halved.

We are aware of the limitations of 2-D DDC simulations as compared to 3-D ones. However, at least for large $Pr \geq 1$, qualitatively the results for 2-D and 3-D are very similar (van der Poel, Stevens & Lohse 2013; Chong *et al.* 2020) and we aim more at elucidating the physical processes originating the layering rather than detailing a specific case. Only by restricting to 2-D, can we explore a large region of the parameter space.

About the initial conditions, the concentration field is linear vertically and the temperature field is linear horizontally. The initial profiles of the scalar fields have also been visualized in the supplementary materials available at https://doi.org/10.1017/jfm.2020.565. For the velocity, the systems are motionless initially, without any perturbation.

https://doi.org/10.1017/jfm.2020.565 Published online by Cambridge University Press

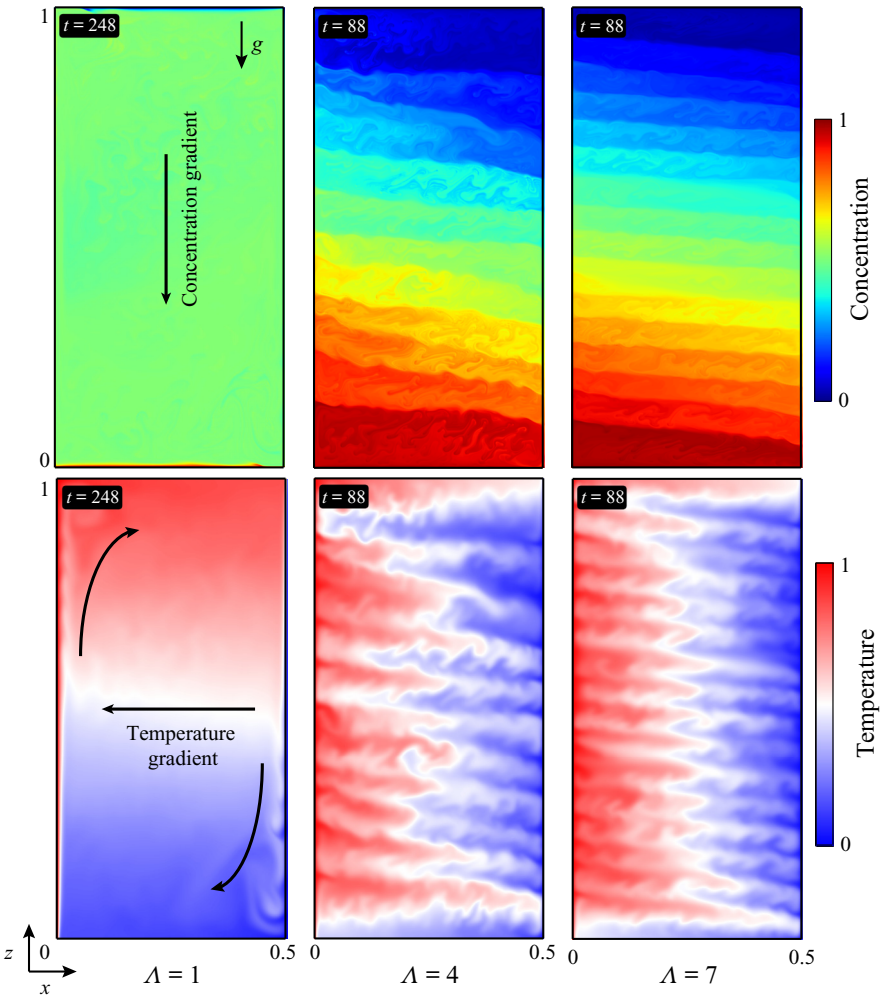


FIGURE 1. Snapshots of the concentration (upper row) and temperature fields (lower row) for different $\Lambda = 1, 4$ and 7 (from left to right) with $Ra_T = 10^9$ and $Le = 100$. The global temperature difference is imposed laterally while the global concentration difference is along the vertical direction to stabilize the flow. Layered structures emerge at large enough density ratio Λ, which contrasts the domain-filling circulation (sketched by arrows) observed at $\Lambda = 1$. Corresponding movies are shown in the supplementary materials.

3. Flow structures at various density ratios

We begin with the qualitative description on how the flow morphology changes with increasing density ratio Λ, where Λ measures the strength of the thermal buoyancy compared to stabilization due to the stable stratification. For this study we fix $Ra_T = 10^9$ and $Le = 100$. In figure 1, we show the concentration and temperature fields for both regimes which emerge.

At $\Lambda = 1$, when the thermal buoyancy is dominant, there is a single large-scale circulation. From the temperature field, it can be seen that the detached hot (cold) plumes travel upwards (downwards). For the chosen aspect ratio $\Gamma = 1/2$, they travel over the distance of the entire cell height. At the same time, the concentration field is advected

https://doi.org/10.1017/jfm.2020.565 Published online by Cambridge University Press

by the thermally-driven circulation. As a result, there is a region formed in the bulk with nearly uniform concentration, whereas the concentration only changes sharply near the top and bottom boundary layers. This flow structure is similar to that in vertical convection VC (Ng *et al.* 2015; Shishkina & Horn 2016; Wang *et al.* 2019). We thus classify this and corresponding cases into the so-called quasi-VC regime.

Strikingly, different flow structures are obtained for Λ larger than a threshold value, which will be calculated in § 4. For example, for $\Lambda = 4$ beyond this threshold, we identify the formation of a layered structure from the concentration field. The physical process of layer formation is as follows: after starting the simulation, there is formation of hot plumes near the hot sidewall, and they travel upwards since they carry lighter fluid than the surroundings. Due to the restoring force caused by the stably stratified concentration field, thermal buoyancy is not strong enough to maintain the upward-moving plumes throughout the entire domain height. Therefore, thermal plumes travel horizontally towards the middle of the cell because of the incompressible condition and conservation of mass, causing a sequence of thermal streaks as seen from the temperature field. In this case, the thermal driving leads to the vertically stacked convection rolls (localized circulations in the clockwise direction), and the convection rolls appear successively from the top and the bottom of the system. Because the concentration diffuses much slower than the heat ($Le = \kappa_T/\kappa_S = 100$), a well-recognizable layered concentration field results. Within each roll, the concentration is nearly uniform due to the convective mixing. At the interface between two adjacent rolls, the concentration changes sharply. For an even larger stabilization ($\Lambda = 7$), even more layers initially form as compared to the case of $\Lambda = 4$, in accordance with our physical explanation of the formation process.

However, when the density ratio Λ is larger than a certain transition value Λ_c, there is no convection. The boundary between the layered regime and the regime without convection has already been obtained by Thorpe *et al.* (1969), which is $\Lambda_c = 0.6Ra_T^{1/5}$.

4. Initial layer thickness and phase space

As shown above, a series of layers (in the concentration field) will form initially in the layered regime, and the initial layer thickness decreases with increasing strength of stabilization. What sets the initial layer thickness or, equivalently, the size of the localized circulation? We will derive this initial layer thickness from an energy balance. A similar energy argument was adopted in stratified Taylor–Couette (TC) flow, which is TC flow subjected to vertical linear stratification (Boubnov, Gledzer & Hopfinger 1995). In stratified TC flow, spontaneous layer formation can be observed in both the low-Re (Boubnov *et al.* 1995) and the high-Re (Oglethorpe, Caulfield & Woods 2013) regimes. In order to estimate the layer thickness in stratified TC flow, Boubnov *et al.* (1995) successfully employed the balance between the work exerted by the centripetal force and the potential energy for moving the fluid parcel in the stable stratification.

Likewise, in laterally cooled DDC, the work for raising the fluid parcel in the stable stratification is done by the thermal buoyancy. As the fluid movement is driven by the horizontal temperature difference Δ_T, the work done by thermal buoyancy to raise the fluid parcel over distance h is $(\beta_T g \Delta_T)h$. In stable linear stratification, the potential energy to bring a fluid parcel out of its equilibrium position with vertical displacement h is $N_0^2 h^2$, where $N_0 = \sqrt{g\beta_s\Delta_s/H}$ is the buoyancy frequency. Assume that all work is converted to potential energy. This balance gives

$$(\beta_T g \Delta_T)h = g\beta_s\Delta_s h^2/H \quad \text{implying} \quad h/H = 1/\Lambda. \tag{4.1}$$

https://doi.org/10.1017/jfm.2020.565 Published online by Cambridge University Press

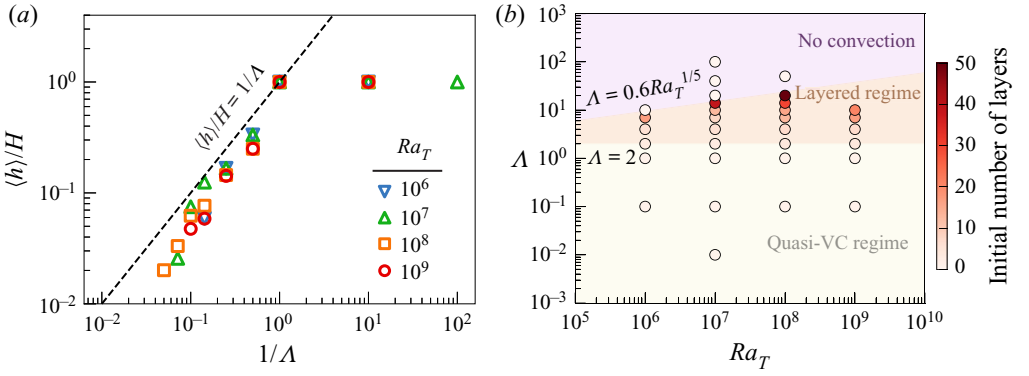


FIGURE 2. (*a*) Normalized average layer thickness $\langle h\rangle/H$ versus $1/\Lambda$ for different Ra_T. The black-dashed line $\langle h\rangle/H = 1/\Lambda$ is derived based on the energy balance discussed in § 4. (*b*) Explored phase space and illustration of different flow regimes. In the quasi-VC regime, the flow resembles that in vertical convection. In the layered regime, layered structures initially emerge. The boundary between the quasi-VC and the layered regime is given by $\Lambda = 2$ as derived by the energy balance in § 4. The boundary between the layered regime and the regime without convection is $\Lambda_c = 0.6Ra_T^{1/5}$ as obtained already by Thorpe *et al.* (1969). The colours of the points denote the number of layers observed in the early stage of the layer formation; later these layers partly merge.

We note that Chen *et al.* (1971) had also introduced this natural length scale to describe the layering pattern in their experiments. We further emphasize that this relationship is only valid for estimating the initial thickness because it assumes a linear stratification which is only the case during the initial stage.

We now check whether (4.1) is a good approximation to the initial layer thickness. We first manually count the number of layers formed in the very initial stage after layer development, which is well recognizable from the snapshots (see for example figure 1). Then the average layer thickness $\langle h\rangle$ can be estimated by dividing the cell height H over the counted number. Figure 2(*a*) shows the evaluated layer thickness $\langle h\rangle/H$ versus $1/\Lambda$ for various Ra_T. It can be seen that the data points generally follow the trend of $h/H = 1/\Lambda$. Yet, close inspection suggests that all data points are actually below the estimated line (black-dashed), consistent with previous experiments, which also found that the measured initial thickness is in general less than $1/\Lambda$ (Chen *et al.* 1971). Analogously, in the studies of double diffusive intrusions (Ruddick & Turner 1979), layers can also form after removing the barrier separating the two different solutions. Besides, there is successive layer formation when ice blocks melt into a salinity gradient (Huppert & Turner 1980). The vertical length scales of the layers in those systems are also found to be proportional to $1/\Lambda$ with the proportionality constant being less than 1. There are two reasons why h/H is smaller than $1/\Lambda$: (i) part of the work is not converted but dissipated which is neglected in obtaining (4.1); (ii) the buoyancy in general is smaller than $\beta_T g\Delta_T$. Thus, (4.1) can only be seen as an upper limit for the initial thickness. In addition, the layer thickness is obviously limited by the system height H, and indeed in figure 2(*a*) it can be seen that $\langle h\rangle$ levels off at $\langle h\rangle = H$ for small $\Lambda \leq 1$ or $1/\Lambda \geq 1$.

We now explore the full parameter space (Λ, Ra_T) to identify when a single large-scale circulation forms, and when there are layers consisting of stacking localized circulations. In figure 2(*b*), the transition boundary between the quasi-VC regime and the layered regime corresponds to the case with only two initially formed layers, i.e. $\Lambda = 2$ from (4.1).

https://doi.org/10.1017/jfm.2020.565 Published online by Cambridge University Press

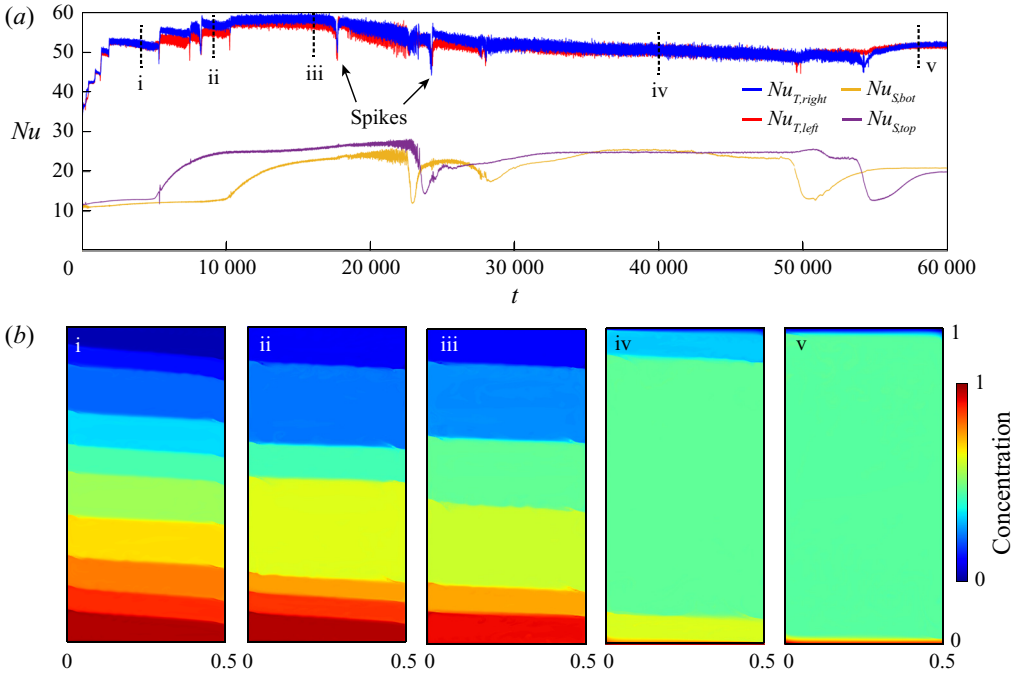


FIGURE 3. (*a*) Time series of the temperature and the concentration Nusselt number, see legend. (*b*) The corresponding concentration field at the marked (in *a*) time instants (i)–(v) are shown.

Upon increasing Λ, the number of layers increases but eventually the system reaches the motionless state when stabilization becomes dominant. This transition density ratio Λ_c to the no convection regime was deduced previously from linear stability analysis (Thorpe *et al.* 1969).

5. Layer merging and its mechanism

We next address the merging of the layers, which successively occurs as time proceeds. It obviously coincides with the number of layers decreasing monotonically with time. Previous experiments had observed an eventual single roll state after successive layer merging (Kamakura & Ozoe 1993) for certain parameters. To study the merging process in detail, we simulated the case of $Ra_T = 10^9$ and $\Lambda = 7$ for 6×10^4 free-fall time units.

Figure 3(*a*) shows the time evolution of the lateral heat flux ($Nu_{T,right}$ and $Nu_{T,left}$) and the vertical solutal flux ($Nu_{S,top}$ and $Nu_{S,bot}$) for this prolonged run; the instantaneous concentration fields at different time instants are also shown in figure 3(*b*). Between the consecutive merging events, the system reaches a meta-stable state with fluxes fluctuating around an average value. However, just before the transition to another meta-stable state (i.e. layer merging), we observe spikes in the heat flux time series which are characteristic of layer merging. After the neighbouring layers have merged, the heat fluxes then reach another average value. In contrast, the solutal fluxes at the top and bottom walls are less sensitive to the merging event as compared to the heat fluxes at sidewalls. The reason is that the response of solutal fluxes to merging events that happen in the interior is delayed. We also note that the step change in the heat fluxes after layer merging has also been reported

https://doi.org/10.1017/jfm.2020.565 Published online by Cambridge University Press

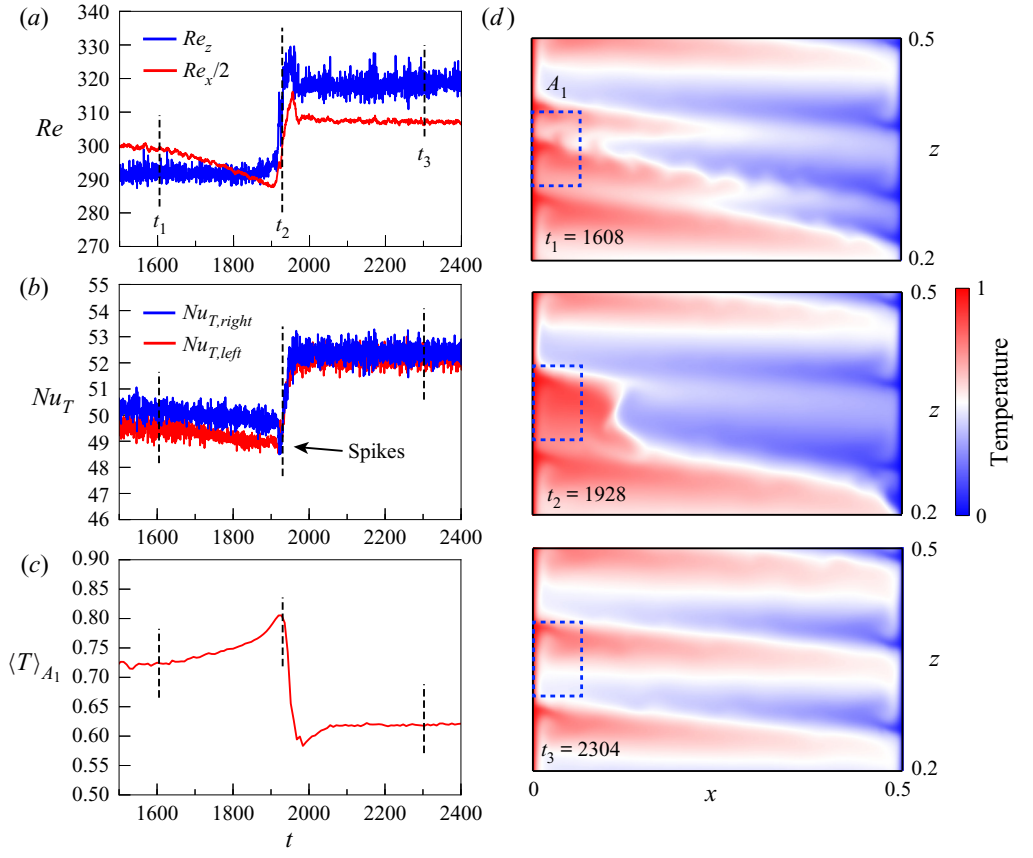


FIGURE 4. Time series of (a) the Reynolds number for the horizontal velocity Re_x and for the vertical velocity Re_z. (b) Time series of the temperature Nusselt number for the left sidewall $Nu_{T,left}$, the right sidewall $Nu_{T,right}$ and (c) the averaged temperature $\langle T\rangle_{A_1}$ over the domain A_1. (d) Portion of the temperature snapshots at these different time instants as marked in (a–c). The extent of the domain A_1 ($0.3 \leq z \leq 0.4$ and $0 \leq x \leq 0.125$), over which $\langle T\rangle_{A_1}$ is averaged in (c), is also sketched.

in the previous numerical work by Nishimura, Kunitsugu & Morega (2000). However, some details have not been discussed, for example, the spikes.

The Nu behaviour leads us to ask: (i) Why are there spikes just before the merging of layers? (ii) What is the merging mechanism in the laterally cooled DDC? To answer these questions, we examine a particular merging event. Figure 4(a) shows the vertical and horizontal Reynolds number, Re_z and Re_x, computed by the globally averaged horizontal and vertical velocities. Between t_1 and t_2, Re_z is almost unchanged, whereas Re_x progressively decreases with time during this period. The weakened horizontal velocity first explains why there is a gradual decrease in lateral heat fluxes shown in figure 4(b).

To study the merging process in even more detail, we visualize the temperature snapshots at the corresponding time instants t_1 and t_2 in figure 4(d). At the moment, when the layers are just about to merge ($t = t_2$), we observe that the thermal streak becomes shorter than before ($t = t_1$), reflecting the weakened local circulation within a layer. Eventually, the weakened circulation leads to an accumulation of hot fluid adjacent to the heated walls. Indeed, in figure 4(c), we see that the averaged temperature over the

https://doi.org/10.1017/jfm.2020.565 Published online by Cambridge University Press

area near the heated wall (denoted by zone A_1) increases gradually before t_2. Finally, when the hot fluid has large enough potential energy to overcome the stable stratification, two nearby layers merge into a larger one at t_3. A new circulation establishes after layer merging; it further carries a chunk of accumulated hot fluid near the heated wall to the opposite cold wall, and subsequently leads to the sharp increase in the heat fluxes. Our results demonstrate the complete process of layer merging in laterally cooled DDC, and further explain why there are spikes in the heat flux time series.

We remark that Radko *et al.* (2014) had studied a merging pattern in thermohaline staircases, in which the interfaces with sharp gradient grow at the expense of interfaces with the smeared out gradient. It is relevant to the merging event observed in our case where the merging is led by the smearing out of the interface. However, the configuration considered here is different from that in Radko *et al.* (2014) with both the concentration and temperature gradients acting in a vertical direction. Such a difference in the configuration can indeed lead to different merging behaviour, for example, the merging instability in our case is triggered in the localized region near the hot sidewall.

6. Concluding remarks

In summary, inspired by the layer formation in café latte, we have numerically studied laterally cooled and stably density stratified DDC, which is regarded as a simplified version of café latte. We have clearly demonstrated the layer formation, which occurs after the initial espresso injection process. We numerically explored large range parameters, namely for the temperature Rayleigh number $10^6 \leq Ra_T \leq 10^9$ and for the density ratio $10^{-2} \leq \Lambda \leq 10^2$, with $Le = 100$.

Upon increasing strength of the stabilizing concentration gradient at a fixed lateral thermal driving, the study reveals the flow transition from the quasi-VC regime to the layered regime. In the quasi-VC regime, the flow structure is a large-scale circulation. However, in the layered regime, multiple localized circulations initially form which, therefore, lead to the layered structure in the concentration field. Based on the energy balance between the work done by thermal buoyancy and the potential energy to bring a fluid parcel out of its equilibrium position in stratification, we can estimate the initial layer thickness, obtaining that it roughly follows $h/H = 1/\Lambda$. Such a relationship also allows us to find the boundary between quasi-VC and layered regimes, which is $\Lambda = 2$.

We finally focused on merging events by running a specific case with a long time series. With sufficiently long simulations, we showed that the layered structures eventually merge into a single large-scale circulation. The merging mechanism is that the weakened circulation within a layer leads to the accumulation of hot fluid over the hot sidewall. The hot fluid parcel at some point obtains enough buoyancy to overcome the energy barrier set by the stable stratification, and it forms a new circulation of larger size. The formation of the new circulation leads to the spikes in the heat flux time series which is characteristic for layer merging.

Until now, we have only considered the cases with fixed temperature at the heated and cooled walls. However, in many circumstances, the DDC may also be subjected to time-dependent boundary conditions, for example, abrupt temperature change caused by falling icebergs, or seasonal temperature variation. Those time-dependent forcings may have a pronounced effect on the layer formation and merging, which is worthy to be studied in the future.

https://doi.org/10.1017/jfm.2020.565 Published online by Cambridge University Press

Acknowledgements

We greatly appreciate the valuable discussions with Y. Li and C. S. Ng. We acknowledge the support from an ERC-Advanced Grant under the project number 740479. K. L. C. acknowledges Croucher Foundation for Croucher Fellowships for Postdoctoral Research. We acknowledge PRACE for awarding us access to MareNostrum 4 based in Spain at the Barcelona Computing Center (BSC) under Prace project 2018194742. We also acknowledge that the results of this research have been achieved using the DECI resource Kay based in Ireland at the Irish Center for High-End Computing (ICHEC) with support from the PRACE aisbl. This work was also partly carried out on the national e-infrastructure of the SURFsara with the support of SURF Cooperative.

Declaration of interests

The authors report no conflict of interest.

Supplementary material and movies

Supplementary material and movies are available at https://doi.org/10.1017/jfm.2020.565.

References

BOUBNOV, B. M., GLEDZER, E. B. & HOPFINGER, E. J. 1995 Stratified circular Couette flow: instability and flow regimes. *J. Fluid Mech.* **292**, 333–358.

CHEN, C. F., BRIGGS, D. G. & WIRTZ, R. A. 1971 Stability of thermal convection in a salinity gradient due to lateral heating. *Intl J. Heat Mass Transfer* **14** (1), 57–65.

CHEN, C. F. & CHEN, F. 1997 Salt-finger convection generated by lateral heating of a solute gradient. *J. Fluid Mech.* **352**, 161–176.

CHONG, K. L., YANG, R., YANG, Y., VERZICCO, R. & LOHSE, D. 2020 Subcritical behaviour in double diffusive convection within the diffusive regime. arXiv:2003.12394.

GARAUD, P. 2018 Double-diffusive convection at low Prandtl number. *Annu. Rev. Fluid Mech.* **50** (1), 275–298.

GAYEN, B., GRIFFITHS, R. W. & KERR, R. C. 2016 Simulation of convection at a vertical ice face dissolving into saline water. *J. Fluid Mech.* **798**, 284–298.

HUPPERT, H. E. & TURNER, J. S. 1980 Ice blocks melting into a salinity gradient. *J. Fluid Mech.* **100** (2), 367–384.

HUPPERT, H. E. & TURNER, J. S. 1981 Double-diffusive convection. *J. Fluid Mech.* **106**, 299–329.

JACOBS, S. S., HUPPERT, H. E., HOLDSWORTH, G. & DREWRY, D. J. 1981 Thermohaline steps induced by melting of the erebus glacier tongue. *J. Geophys. Res.* **86** (C7), 6547–6555.

JOHNSON, G. C. & KEARNEY, K. A. 2009 Ocean climate change fingerprints attenuated by salt fingering? *Geophys. Res. Lett.* **36** (21), 1–5.

KAMAKURA, K. & OZOE, H. 1993 Experimental and numerical analyses of double diffusive natural convection heated and cooled from opposing vertical walls with an initial condition of a vertically linear concentration gradient. *Intl J. Heat Mass Transfer* **36** (8), 2125–2134.

KELLEY, D. E., FERNANDO, H. J. S., GARGETT, A. E., TANNY, J. & ÖZSOY, E. 2003 The diffusive regime of double-diffusive convection. *Prog. Oceanogr.* **56** (3-4), 461–481.

LEE, J. W. & HYUN, J. M. 1991 Double diffusive convection in a cavity under a vertical solutal gradient and a horizontal temperature gradient. *Intl J. Heat Mass Transfer* **34** (9), 2423–2427.

MENDENHALL, C. E. & MASON, M. 1923 The stratified subsidence of fine particles. *Proc. Natl Acad. Sci.* **9** (6), 199–202.

https://doi.org/10.1017/jfm.2020.565 Published online by Cambridge University Press

NG, C. S., OOI, A., LOHSE, D. & CHUNG, D. 2015 Vertical natural convection: application of the unifying theory of thermal convection. *J. Fluid Mech.* **764**, 349–361.

NISHIMURA, T., KUNITSUGU, K. & MOREGA, AL. M. 2000 Direct numerical simulation of layer merging in a salt-stratified system. *Numer. Heat Transfer* A **37** (4), 323–341.

OGLETHORPE, R. L. F., CAULFIELD, C. P. & WOODS, A. W. 2013 Spontaneous layering in stratified turbulent Taylor–Couette flow. *J. Fluid Mech.* **721**, R3.

OSTILLA-MÓNICO, R., YANG, Y, VAN DER POEL, E. P., LOHSE, D. & VERZICCO, R. 2015 A multiple-resolution strategy for direct numerical simulation of scalar turbulence. *J. Comput. Phys.* **301**, 308–321.

VAN DER POEL, E. P., OSTILLA-MÓNICO, R., DONNERS, J. & VERZICCO, R. 2015 A pencil distributed finite difference code for strongly turbulent wall-bounded flows. *Comput. Fluids* **116**, 10–16.

VAN DER POEL, E. P., STEVENS, R. J. A. M. & LOHSE, D. 2013 Comparison between two-and three-dimensional Rayleigh–Bénard convection. *J. Fluid Mech.* **736**, 177–194.

RADKO, T. 2013 *Double-Diffusive Convection*. Cambridge University Press.

RADKO, T., FLANAGAN, J. D., STELLMACH, S. & TIMMERMANS, M.-L. 2014 Double-diffusive recipes. Part 2. Layer-merging events. *J. Phys. Oceanogr.* **44** (5), 1285–1305.

RUDDICK, B. R. & TURNER, J. S. 1979 The vertical length scale of double-diffusive intrusions. *Deep-Sea Res.* **26** (8), 903–913.

SCHMITT, R. W. 1994 Double diffusion in oceanography. *Annu. Rev. Fluid Mech.* **26** (1), 255–285.

SCHMITT, R. W. 2005 Enhanced diapycnal mixing by salt fingers in the thermocline of the tropical Atlantic. *Science* **308** (5722), 685–688.

SHISHKINA, O. & HORN, S. 2016 Thermal convection in inclined cylindrical containers. *J. Fluid Mech.* **790**, R3.

SIMEONOV, J. & STERN, M. 2004 Double-diffusive intrusions on a finite-width thermohaline front. *J. Phys. Oceanogr.* **34** (7), 1723–1740.

SOMMER, T., CARPENTER, J. R., SCHMID, M., LUECK, R. G., SCHURTER, M. & WÜEST, A. 2013 Interface structure and flux laws in a natural double-diffusive layering. *J. Geophys. Res.* **118** (11), 6092–6106.

TANNY, J. & TSINOBER, A. B. 1988 The dynamics and structure of double-diffusive layers in sidewall-heating experiments. *J. Fluid Mech.* **196**, 135–156.

THORPE, S. A., HUTT, P. K. & SOULSBY, R. 1969 The effect of horizontal gradients on thermohaline convection. *J. Fluid Mech.* **38** (2), 375–400.

TIMMERMANS, M. L., TOOLE, J., KRISHFIELD, R. & WINSOR, P. 2008 Ice tethered profiler observations of the double diffusive staircase in the Canada basin thermocline. *J. Geophys. Res.* **113**, 0–02.

TURNER, J. S. 1974 Double diffusive phenomena. *Annu. Rev. Fluid Mech.* **6** (1), 37–56.

VERZICCO, R. & ORLANDI, P. 1996 A finite-difference scheme for three-dimensional incompressible flows in cylindrical coordinates. *J. Comput. Phys.* **123** (2), 402–414.

WANG, Q., XIA, S.-N., YAN, R., SUN, D.-J. & WAN, Z.-H. 2019 Non-Oberbeck-Boussinesq effects due to large temperature differences in a differentially heated square cavity filled with air. *Intl J. Heat Mass Transfer* **128**, 479–491.

WIRTZ, R. A., BRIGGS, D. G. & CHEN, C. F. 1972 Physical and numerical experiments on layered convection in a density-stratified fluid. *Geophys. Fluid Dyn.* **3** (1), 265–288.

XUE, N., KHODAPARAST, S., ZHU, L., NUNES, J. K., KIM, H. & STONE, H. A. 2017 Laboratory layered Latte. *Nat. Commun.* **8** (1960), 1–6.

YANG, Y., VERZICCO, R. & LOHSE, D. 2015 From convection rolls to finger convection in double-diffusive turbulence. *Proc. Natl Acad. Sci.* **113** (1), 69–73.

YANG, Y., CHEN, W., VERZICCO, R. & LOHSE, D. 2020 Multiple states and transport properties of double-diffusive convection turbulence. *Proc. Natl Acad. Sci.* **117** (26), 14676–14681.

https://doi.org/10.1017/jfm.2020.565 Published online by Cambridge University Press